Eigenmodes for the inversion of 3D electromagnetic data

C. Stuntebeck, Institute of Geophysics and Meteorology, TU Braunschweig (c.stuntebeck@tu-bs.de)

Abstract

The term 'eigenmodes' refers to the modes of freely-decaying currents in a conductor. Taking advantage of the eigenmodes offers an efficient method of calculating electromagnetic field responses over 3D conductivity structures as well as their sensitivity to variations in conductivity. In this article, we shall sketch the theoretical basics of the eigenmodes, describe how their numerical determination is realised, and depict some characteristic eigenmodes. We introduce the newly developed procedure of 3D modelling based on an approximate, partial eigenmode expansion. Its performance is discussed considering an airborne survey above a conductive 3D body. Furthermore, the relevance of the eigenmodes for the inversion of 3D EM data is presented.

A more detailed investigation of the eigenmode approach is given in Stuntebeck (2003).

Free-decay eigenmodes

The process of electromagnetic induction is governed by Maxwell's equations,

$$\nabla \times \underline{E}(\underline{r}) = -\dot{\underline{B}}(\underline{r}), \qquad \nabla \times \underline{B}(\underline{r}) = \mu_0 \left[\sigma(\underline{r})\underline{E}(\underline{r}) + \underline{J}^e(\underline{r})\right]. \tag{1}$$

In these expressions $\underline{r}$ is the vector of position, $\underline{E}(\underline{r})$ and $\underline{B}(\underline{r})$ are the vectors of the electric and magnetic field, and $\sigma(\underline{r})$ denotes the electric conductivity. $\underline{J}^e(\underline{r})$ is the source current density. The dotted variables signify time derivatives. After elimination of $\underline{B}$, the induction equation

$$\nabla \times \nabla \times \underline{E}(\underline{r}) + \mu_0 \sigma(\underline{r}) \dot{\underline{E}}(\underline{r}) = -\mu_0 \dot{\underline{J}}^e(\underline{r}) \tag{2}$$

is obtained. The free-decay of currents takes places in the absence of an exciting source, for which equation (2) reduces to

$$\nabla \times \nabla \times \underline{E}(\underline{r}) + \mu_0 \sigma(\underline{r}) \dot{\underline{E}}(\underline{r}) = 0. \tag{3}$$

Since the time dependence does not occur in the coefficients, it can be split-off by an exponential factor,

$$\underline{E}(\underline{r}, t) = \underline{e}(\underline{r}) \exp(-\lambda t), \tag{4}$$

such that (3) leads to the eigenvalue problem

$$\nabla \times \nabla \times \underline{e}(\underline{r}) = \lambda \mu_0 \sigma(\underline{r}) \underline{e}(\underline{r}) \tag{5}$$

with the non-negative decay constant λ as eigenvalue of the vectorial eigenfunction $\underline{e}(\underline{r})$.

The set of solutions to (5) contains also spurious modes, which are associated with $\lambda = 0$ and exhibit an unphysically divergent current density. To exclude these spurious modes, the eigenvalue problem (5) has to be solved incorporating the side condition

$$\nabla \cdot \left[\sigma(\underline{r})\, \underline{e}(\underline{r})\right] = 0. \tag{6}$$

If the numerical solution of the conditioned eigenvalue problem, as defined by (5) and (6), is

carried out for a bounded volume of the conductor, one obtains a finite set of discrete eigenfunctions. The discrete eigenfunctions $\underline{e}_n$ of the electric field fulfill the weighted orthogonality relation

$$\int_V \sigma(\underline{r})\ \underline{e}_k(\underline{r})\ \underline{e}_n(\underline{r})\ \mathrm{d}^3\underline{r} = \delta_{kn}. \tag{7}$$

The set of all discrete eigenfunctions and -values $\{\underline{e}_n, \lambda_n\}$ forms a complete set of functions in the conductor where $\sigma > 0$. Therefore, here any electric field in frequency domain can be expanded in terms of the eigenmodes

$$\underline{E}(\underline{r}, \omega) = \sum_n a_n(\omega)\underline{e}_n(\underline{r}), \tag{8}$$

where the expansion coefficients a_n contain the field source frequency ω and current density $\underline{J}^e(\underline{r})$

$$a_n = -\frac{i\omega}{\lambda_n + i\omega} \int_V \underline{J}^e(\underline{r}) \cdot \underline{e}_n(\underline{r})\ \mathrm{d}^3\underline{r}. \tag{9}$$

In particular, the expansion coefficients for a vertical magnetic dipole (VMD) at position $\underline{r}_T$ with moment m read

$$a_n = -\frac{i\omega}{\lambda_n + i\omega}\ m\left[\nabla \times \underline{e}_n(\underline{r}_T)\right]_z. \tag{10}$$

The associated electric field of a VMD with observation point $\underline{r}$ and $\underline{r}_T$ placed in the air half space is given by

$$\underline{E}(\underline{r}|\underline{r}_T, \omega) = \underline{E}_\infty(\underline{r}|\underline{r}_T, \omega) - i\omega m \sum_n \frac{\underline{e}_n(\underline{r})\left[\nabla \times \underline{e}_n(\underline{r}_T)\right]_z}{\lambda_n + i\omega}. \tag{11}$$

In this case the eigenmode expansion is incomplete. The supplementary term $\underline{E}_\infty(\underline{r}|\underline{r}_T, \omega)$ accounts for the non-vanishing field in the air in the limit $\omega \to \infty$, when all conducting material acts like a perfect conductor (in which all fields vanish) and the field in the air half space is simply given by the source field and its mirror source, reflected at the earth-air interface.

Numerical determination of the eigenmodes

For the practical implementation of the eigenvalue problem we use finite differences on a staggered grid, which is composed of N grid cells with uniform conductivity inside each cell. The FD system equations are set up only in terms of the three electric field components, which yields a set of $\sim 3 \cdot N$ equations. The resulting equations as well as the employed boundary conditions are explicitly stated in Stuntebeck (2002). Taking into account the side condition (6) in FD yields an additional equation at each internal grid node. Since the number of FD side equations corresponds to the number of non-trivial vertical electric components e_z, they can be used to eliminate e_z from the original FD eigenvalue problem. The resulting reduced set of equations is based only on the horizontal electric components e_x and e_y, which are combined in the vector $\check{\mathbf{e}}$. The associated system matrix $\boldsymbol{B}$ is still high-dimensional ($N_B \sim 2 \cdot N$), real, and sparse, but now has become non-symmetric and positive definite. The latter implies the important property that now all eigenvalues are positive, $\lambda > 0$, and that the respective eigenmodes are all real non-spurious modes.

The FD eigenvalue problem $\boldsymbol{B}\check{\mathbf{e}} = \lambda\check{\mathbf{e}}$ is solved using the Implicitly Restarted Arnoldi Method (IRAM) of ARPACK (Lehoucq et al., 1998). This progam package allows for the efficient determination of arbitrary parts of the discrete set of eigenmodes $\{\check{\mathbf{e}}_n, \lambda_n\}$, $n = 1, \ldots, N_B$.

Exemplary eigenmodes

A typical eigenvalue spectrum is given in Figure 1. It is determined for a uniform box with a resistivity of 100 Ωm. The box is divided into $16 \times 16 \times 8$ cells. Accordingly, the eigenvalue problem is of dimension $N_B = 3840$.

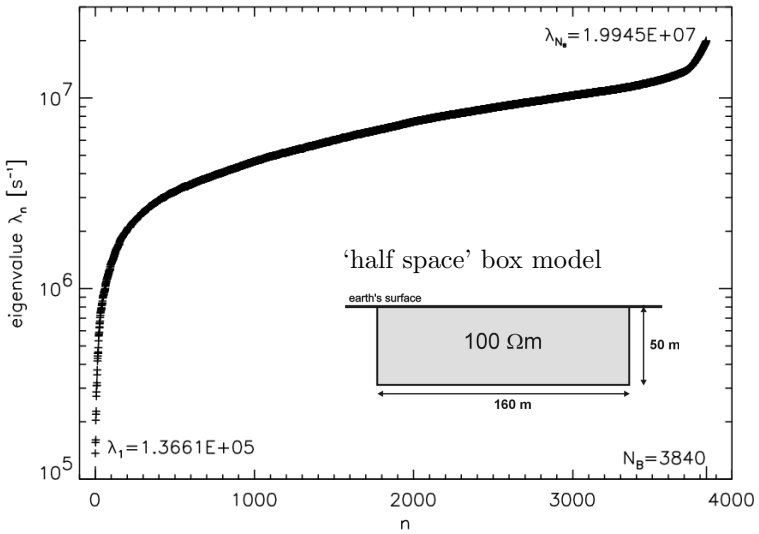

Figure 1: Eigenvalue spectrum of a 100 Ωm 'half space' box constisting of 2048 cells.

The discrete eigenvalues vary in the range

$$\lambda_{min} := \frac{c_1\ \pi^2}{\mu_0\ \sigma_{max}\ L_{max}^2} \leq \lambda_n \leq \frac{c_2\ \pi^2}{\mu_0\ \sigma_{min}\ L_{min}^2} =: \lambda_{max}, \tag{12}$$

with the constants $c_1,\ c_2 \approx 1 - 10$, the extrema of conductivity σ_{min}, σ_{max}, the smallest length of discretisation L_{min}, and L_{max} being the largest model dimension. The latter primarily determines the smallest eigenvalues. Thus, the smallest decay constants describe slowly decaying eddies of model size, which represent large scale conductivity structures and therefore are the most interesting ones.

Some of these eigenmodes belonging to the smallest eigenvalues are displayed in Figure 2 for a 3D conductivity structure. The modes exhibit a nice symmetry with respect to the embedded conducting block. The modes of different eigenvalues represent different parts of the conductivity structure. How these modes contribute to the field synthesis shall be discussed in the following.

3D EM modelling using eigenmodes

After the numerical solution of the eigenvalue problem, the discrete set of eigenmodes $\{\underline{e}_n, \lambda_n\}$ is available for the 3D conductivity structure under investigation. Once the eigenmodes are known, any arbitrary EM field response can be obtained through a straightforward superposition of the eigenmodes at low computational cost, which simply is repeated for each used frequency ω as well as transmitter and receiver position $\underline{r}_T, \underline{r}_R$.

The expansion for the electric field is given in (11). Using $\underline{B} = -\frac{1}{i\omega}\ \nabla_{\underline{r}_R} \times \underline{E}$, a similar expression is obtained for the magnetic field. In particular, the vertical magnetic field component of a VMD is given by

$$B_{zz}(\underline{r}_R|\underline{r}_T, \omega) = B_{zz,\infty}(\underline{r}_R|\underline{r}_T) + m \sum_{n=1}^{N_B} \frac{[\nabla \times \underline{e}_n(\underline{r}_R)]_z\, [\nabla \times \underline{e}_n(\underline{r}_T)]_z}{\lambda_n + i\omega}, \tag{13}$$

where again the analytic term $B_{zz,\infty}$ accounts for the non-vanishing field in the air in the limit $\omega \to \infty$. Remarkably, the field expansion is based only on the eigenmodes at position of transmitter and receiver.

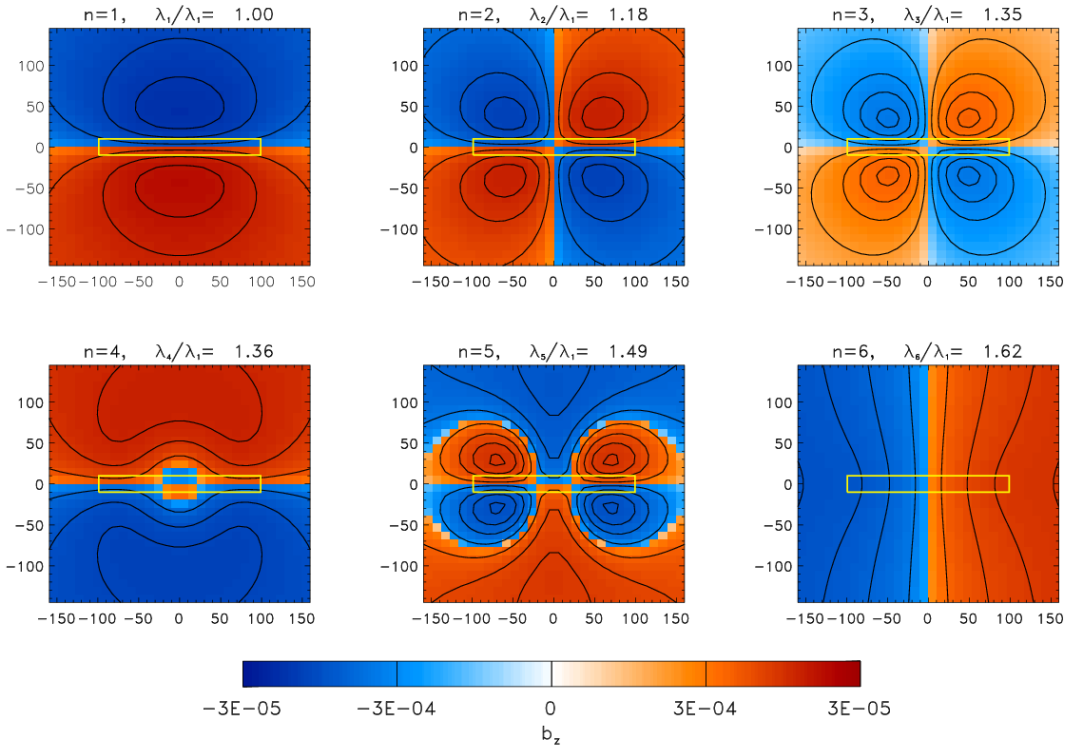

Figure 2: Vertical magnetic eigenmodes $b_{nz} = \frac{1}{\lambda_n}[\nabla \times \underline{e}_n]_z$ at the earth's surface associated with the six smallest eigenvalues, observed for a 1 Ωm 3D body (indicated by yellow line) in an otherwise uniform 100 Ωm box.

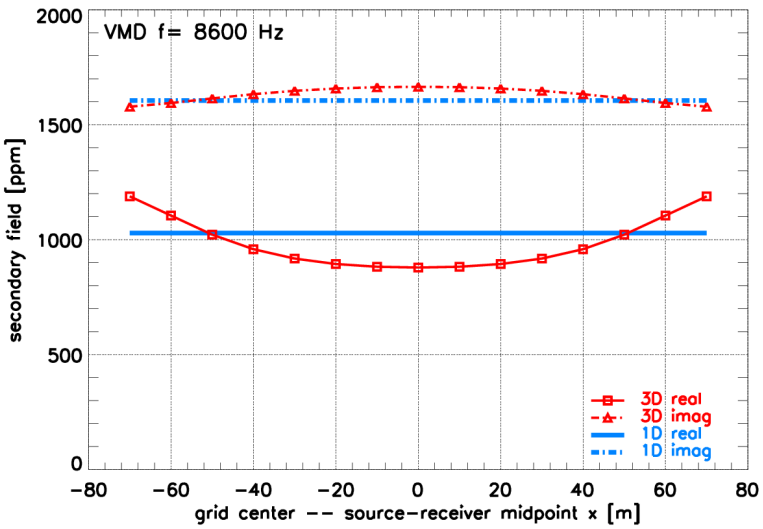

Figure 3: Real and imaginary part of secondary magnetic field along a flight line at $h = 20\,\mathrm{m}$ with fixed transmitter-receiver separation of 10 m above a uniform 100 Ωm box (168 m × 160 m × 50 m). The 3D response (red) is obtained from the synthesis of $N_B = 3840$ eigenmodes. For comparison, the analytic 1D response of the corresponding layered half space is added in blue.

The result of such an eigenmode synthesis is given in Figure 3 along a flight line at 20 m height above a uniform 100 Ωm box. There is an acceptable agreement of the 3D eigenmode response with the analytic 1D response of the corresponding layered half space. The deviations are boundary effects, which are caused by the close lateral boundaries of the small box in comparision to the infinitely extending half space.

However, using this simple model for which an analytic reference solution exists, we derived three alternative formulations of the eigenmode synthesis (13):

1. Straightforward synthesis S1

$$B_{zz}^{S1} = B_{zz,\infty} + m \sum_{n=1}^{n_T} \frac{1}{\lambda_n + i\omega} \left[\nabla \times \underline{e}_n^R\right]_z \left[\nabla \times \underline{e}_n^T\right]_z . \tag{14}$$

2. Synthesis S2 with separated magnetostatic part ($\omega = 0$)

$$B_{zz}^{S2} = \underbrace{B_{zz,\infty} + B_{zz,0}}_{|} - m \sum_{n=1}^{n_T} \frac{i\omega/\lambda_n}{\lambda_n + i\omega} \left[\nabla \times \underline{e}_n^R\right]_z \left[\nabla \times \underline{e}_n^T\right]_z . \tag{15}$$

$B_{zz}(\omega = 0)$ magnetostatic field, calculated by aid of mirror dipoles

3. Synthesis S3 with separated ($\omega = 0$) and frequency proportional part

$$B_{zz}^{S3} = B_{zz}(0) + i\omega \underbrace{B_{zz}^{i\omega}}_{|} + m \sum_{n=1}^{n_T} \frac{(i\omega/\lambda_n)^2}{\lambda_n + i\omega} \left[\nabla \times \underline{e}_n^R\right]_z \left[\nabla \times \underline{e}_n^T\right]_z . \tag{16}$$

frequency proportional term, determined by Biot-Savart

Through separation of the (quasi-)analytical parts of the synthesis, we achive an improved agreement with the 1D response, since the analytic determination of the separated terms is not restricted to the box model but may also be calculated for the half space model. Even more important is the enhanced convergence of the optimised expansion (16). The modified expansion coefficient decreases much faster for increasing eigenvalues, such that the respective eigenmodes yield only minor contributions to the expansion. Thus, a truncation of the expansion after n_T of the smallest eigenvalues becomes feasible without a significant loss in accuracy.

Such a partial synthesis is considered to be a good approximate method to determine the field response, as is demonstrated in Figure 4. The partial synthesis allows the investigation of larger grids due to the reduced numerical effort. For example, the memory and computational time requirements of a partial synthesis with the fraction $n_T = 1/8 N_B$ of all eigenmodes, performed for a $24 \times 24 \times 8$ grid, are similar to those of the full synthesis for a smaller $16 \times 16 \times 8$ grid, see Table 1. For the horizontally enlarged grid, a much better agreement of the 3D partial synthesis with the 1D response is observed, which is due to less influence of the lateral box walls.

After optimisation of the synthesis using the simple uniform conductivity model, we now demonstrate the capabilities of the approximate eigenmode modelling method for a truly three-

grid	N_B	n_T	memory	CPU time	synthesis type
$24\times24\times8$	8832	1104	498 Mb	4.84 h	partial
$16\times16\times8$	3840	3840	490 Mb	3.25 h	full
$16\times16\times8$	3840	480	101 Mb	0.36 h	partial

Table 1: Computational effort for determintion of eigenmodes of small and enlarged grid using full and partial synthesis, for Alpha EV6.7 (21264A) processor operating at 667MHz.

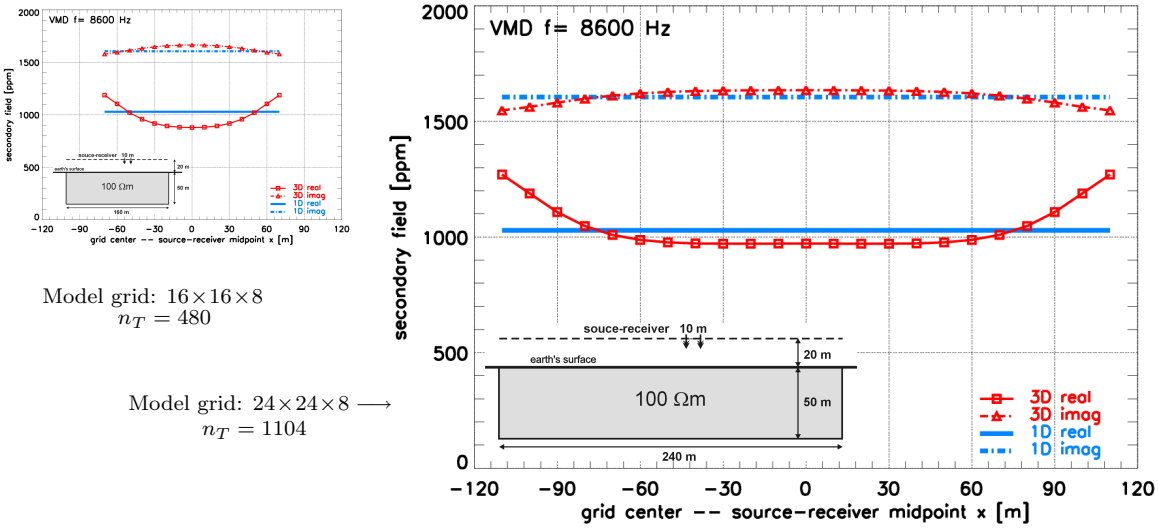

Model grid: $16 \times 16 \times 8$
$n_T = 480$

Model grid: $24 \times 24 \times 8 \longrightarrow$
$n_T = 1104$

Figure 4: Partial synthesis with $n_T = 480$ for the previous small grid (Figure 3) of size 160 m × 168 m × 50 m (left) and $n_T = 1104$ for a horizontally enlarged model of size 240 m × 252 m × 50 m.

dimensional conductivity structure. In this case, there exists no analytic reference solution, therefore we compare our results with the direct FD modelling of Newman and Alumbaugh (1995), as displayed in Figure 5.

Investigated is the airbore ($h = 20$ m) electromagnetic response of a VMD with $f = 900$ Hz at a fixed receiver distance of 10 m along a flight line across a 3D conductive body (1 Ωm) embedded

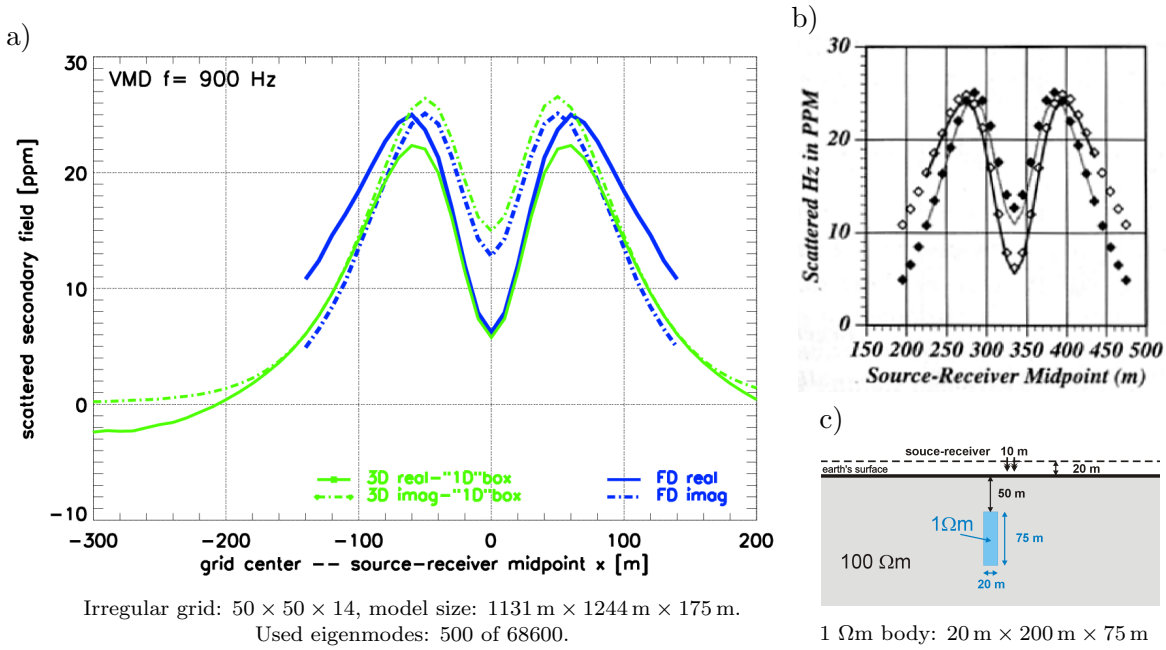

Irregular grid: 50 × 50 × 14, model size: 1131 m × 1244 m × 175 m.
Used eigenmodes: 500 of 68600.

1 Ωm body: 20 m × 200 m × 75 m

Figure 5: Scattered secondary field from partial eigenmode modelling (3D-"1D"box) in a) in direct comparison with the results of Newman and Alumbaugh (1995) (FD). Their original solution is reproduced in b). The measuring configuration and the model of the 3D conductivity structure are stated in c).

Eigenmode modelling

Determination of 500 eigenmodes of B

IRAM	regular	shift & invert
iterativ solver	-	BCGSTAB
preconditioner	-	ILUD
memory	1.6 GB	2.0 GB
CPU time*	22.1 h	15.9 h

Partial synthesis with 500 eigenmodes

number: 51 positions
memory: 1.0 GB
CPU time*: 12 minutes

*Alpha EV6.7 (21264A) processor with 667 MHz

$\Longrightarrow$ 15.9 h + 14 seconds for each forward problem

FD modelling

Newman & Alumbaugh (1995):
number: 29 positions
memory: 120 MB
CPU time: 13.6 h

$\Longrightarrow \sim$ 0.5 h for each forward problem

Table 2: Computational effort of the eigenmode modelling method in comparison to the direct FD modelling of Newman and Alumbaugh (1995).

in a 100 Ωm surrounding. The plotted scattered secondary field is the response of solely the 3D body with the field response of the uniform background removed. Accordingly, we expect vanishing fields at larger distances from the grid center where the body is located. This behaviour is achieved very well for the imaginary part, whereas the real part of the response exibits a small offset of about 2 ppm. Of almost the same size is the maximum deviation between eigenmode and FD modelling along the flight line, however, directly above the anomalous structure a very good agreement of both resonses can be observed. These modelling resuls are considered to be very good, taking into account the approximate nature of the method and the numerical inaccuracies involved with any FD solution.

After we have gained confidence in the principle functioning of the eigenmode modelling method, let us investigate its efficiency, discussing the numerical challenges for the example of Figure 5.

The use of a $50 \times 50 \times 14$ grid leads to an eigenvalue problem with dimension in the order of 10^5, which is unmanagable with classical methods, since the memory to store either the system matrix or all eigenmodes would exceed 35 GB. Making use of the sparseness of the matrix reduces its storage needs to about 300 MB. However, the most important parameter is the memory requirement for each eigenmode, which is $\sim$ 1 MB. This shows the significance of the partial synthesis, since without restriction to only a few eigenmodes the method would not be practicable. In Table 2, the numerical effort of the eigenmode modelling is compared with the FD modelling of Newman and Alumbaugh (1995), which however was performed 8 years ago. The FD modelling requires much less memory, and even the computational time for this example is almost the same which is required to just solve the eigenvalue problem, even with a quite sophisticated method using IRAM in shift & invert mode. However, whereas the FD modelling time shows a linear dependence on the number of forward problems solved, with each problem taking about half an hour, the eigenmode modelling shows an excellent performance, where for each forward problem only an additional time of 14 seconds is required once the eigenmodes are available.

This feature of the eigenmode modelling method allows us for the first time, to simulate the responses of a whole survey in a resonable time, see Figure 6. In this simulation, we modelled the VMD responses along 40 flight lines with each 50 transmitter-receiver positions for 6 frequencies (380 Hz, 900 Hz, 1.8 kHz, 8.6 kHz, 41 kHz, 192 kHz), thus a total of 12000 EM responses. The conductivity model was described by an irregular grid with $50 \times 50 \times 20$ cells. The determination of 500 eigenmodes associated with the smallest eigenvalues of the eigenvalue problem with dimension

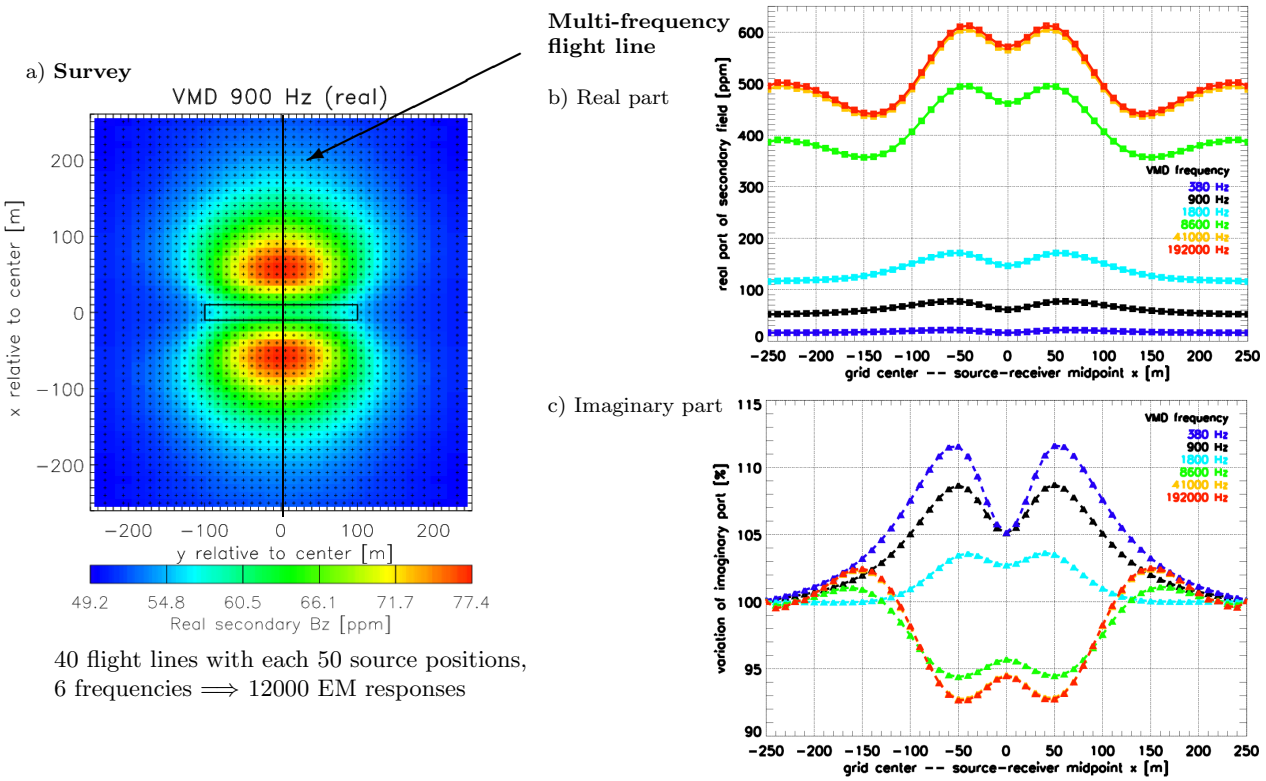

Figure 6: Simulation of a flight survey above the conductive 3D body, as defined in Figure 5 c). In a), for an area of 500 m × 500 m the real part response at $f = 900$ Hz is displayed. The multi-frequency responses along a representative central flight line across the body are given in b) for the real and in c) for the imaginary part.

98000 using IRAM took 21.4 hours. Based on those 500 eigenmodes, the field synthesis for all 12000 EM responses required only an additional time of 1.25 hours. Altogether, we come up to the outstandingly low average computation time of only 7 seconds for each 3D forward modelling.

Inversion based on the eigenmodes

The newly developed modelling method based on a partial expansion in terms of the free-decay eigenmodes turned out to yield an efficient forward operator in 3D modelling. This property makes the eigenmodes attractive for use in an inversion procedure.

Furthermore, the eigenmodes offer a new way of calculating the sensitivities, which are needed to describe how the data change when small perturbations are made to the model during the inversion procedure. In analogy to the field response determination, also the sensitivities can be calculated using a straightforward expansion in terms of the eigenmodes.

The basis of the inversion is an iterative optimisation algorithm to generate the desired earth model which satisfactorily reproduces the measured data, starting from the computed response of an inital model and its associated sensitivities.

We employ the Marquardt method, which essentially consists of an iterative improvement of an estimated starting parameter vector $\mathbf{x}_0 \in \mathbb{R}^N$, where N is the number of parameters, which is performed in k steps until the diminishing vector of data residuals $\mathbf{r}_k \in \mathbb{R}^M$ indicates a sufficient agreement between measured data $\mathbf{y}^{obs} \in \mathbb{R}^M$ and modelled data $\mathbf{y}_k \in \mathbb{R}^M$, where M is the number of data used in the inversion. As long as the parameter vector $\mathbf{x}_k$ yields no satisfactory

response, the next $(k+1)$ approximation is calculated from

$$\mathbf{x}_{k+1} = \mathbf{x}_k + \left(\boldsymbol{S}_k^{\mathrm{T}} \boldsymbol{S}_k + \mu^2 \boldsymbol{I}_N \right)^{-1} \boldsymbol{S}_k^{\mathrm{T}} \mathbf{r}_k, \tag{17}$$

with μ^2 being the regularisation parameter of Marquardt and $\boldsymbol{S}_k \in \mathbb{R}^M \times \mathbb{R}^N$ the sensitivity or Jacobian matrix of iteration k. The elements of the sensitivity matrix are defined as

$$S_{ljk} := \frac{\partial f_l(\mathbf{x}_k)}{\partial x_{jk}} \tag{18}$$

with $f_l(\mathbf{x}_k)$ being the functional to obtain data l belonging to the conductivity model of parameter vector $\mathbf{x}_k$.

The elements of $\boldsymbol{S}_k$ can be determined at low computational cost if the free-decay modes of the model $\mathbf{x}_k$ are known: Using the volume integral equation method, one can derive that small variations in conductivity $\delta\sigma(\underline{r}')$ cause small variations

$$\delta B_{zz}(\underline{r}_R|\underline{r}_T,\omega) = -\frac{1}{i\omega m} \int_V \delta\sigma(\underline{r}')\, \underline{E}(\underline{r}'|\underline{r}_R,\omega) \cdot \underline{E}(\underline{r}'|\underline{r}_T,\omega)\ \mathrm{d}^3\underline{r}' \tag{19}$$

of the vertical component of the VMD magnetic field. If the variations of σ are confined to a single grid cell at $\underline{r}_j$, it follows for the sensitivity of data l

$$S_{lj} = -\frac{1}{i\omega^l m}\, \sigma(\underline{r}_j) V(\underline{r}_j)\ \underline{E}(\underline{r}_j|\underline{r}_R^l,\omega^l) \cdot \underline{E}(\underline{r}_j|\underline{r}_T^l,\omega^l), \tag{20}$$

where according to (11) the electric fields in the conductor (at $\underline{r}_j$) are solely given by

$$\underline{E}(\underline{r}'|\underline{r},\omega) = -i\omega m \sum_n \frac{\underline{e}_n(\underline{r}')\, [\nabla \times \underline{e}_n(\underline{r})]_z}{\lambda_n + i\omega}, \tag{21}$$

an expansion in terms of the eigenmodes $\underline{e}_n$. The required eigenmodes (at position of transmitter, receiver and grid cell) are already known and available from the forward modelling.

The above described inversion algorithm with forward modelling and sensitivity calculation based on a partial expansion in terms of the eigenmodes has been applied for a very simple conductivity model, as shown in Figure 7. The model consists of four parameter blocks, of which one block has an increased resistivity of 300 Ωm while the other three have 100 Ωm.

Starting model for the inversion is a uniform half space with 50 Ωm. The course of the inversion is depicted by the RMS error and the Marquardt parameter (upper panel) as well as the four parameter values (lower panel), plotted versus the overall number of iteration steps. The dotted vertical lines indicate the performed recalculations of the sensitivity matrix.

The inversion yields a parameter modell which reproduces the true resistivity model very well. Remarkably, this was achieved even though the algorithm is based on an approximate determination of the sensitivities, using only a small subset of the eigenmodes.

Therefore, the eigenmodes are a promising approach when aiming at developing an efficient inversion technique for 3D electromagnetic data.

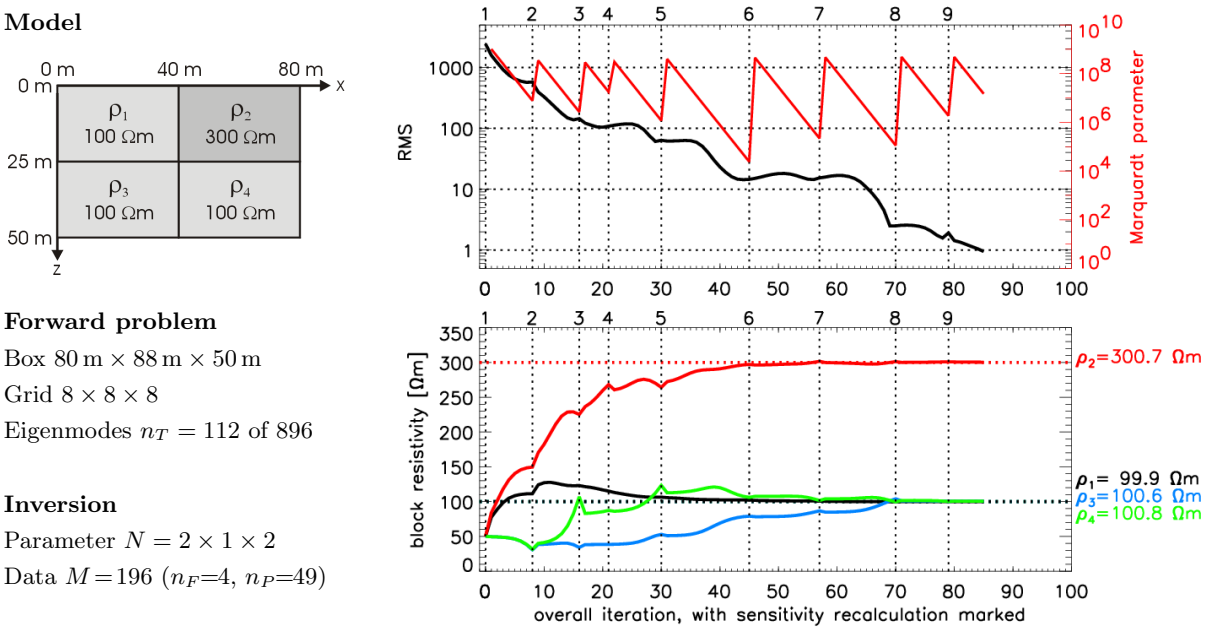

Figure 7: Inversion over a block structure with $\rho_2 = 300$ Ωm and three surrounding blocks with $\rho_{1,3,4} = 100$ Ωm in a box of 80 m × 88 m × 50 m. The inversion is performed on a grid with $N = 2 \times 1 \times 2$ block parameters. The achieved RMS as well as the used value of the Marquardt parameter versus overall iteration is plotted in the upper panel, and likewise the associated four resistivity parameters are displayed below.

Acknowledgements

I would like to thank P. Weidelt for his suggestion and encouraging support of the work as well as for contributing some constitutive parts of the code. The project is funded by the Deutsche Forschungsgemeinschaft (WE 1048/7-1 and WE 1048/7-2).

References

Lehoucq, R. B., Sorensen, D. C. and Yang, C., 1998. *ARPACK Users' Guide: Solution of Large-Scale Eigenvalue Problems with Implicitly Restarted Arnoldi Methods*. SIAM, Philadelphia, PA.
URL `http://www.caam.rice.edu/software/ARPACK/`

Newman, G. A. and Alumbaugh, D. L., 1995. Frequency domain modelling of airborne electromagnetic responses using staggered finite differences. *Geophysical Prospecting* **43**, 1021–1042.

Stuntebeck, C., 2002. First attempts in 3D frequency-domain modelling of electromagnetic responses using eigenmodes. In A. Hördt and J. Stoll (editors), *Protokoll Kolloquium 'Elektromagnetische Tiefenforschung'*, pages 139–151, Deutsche Geophysikalische Gesellschaft, Hannover.

Stuntebeck, C., 2003. *Three-dimensional electromagnetic modelling by free-decay mode superposition*. Ph.D. thesis, Technische Universität Braunschweig.
URL `http://opus.tu-bs.de/opus/volltexte/2003/492/`